

UCSF

UC San Francisco Previously Published Works

Title

Inhibition of Calcium Dependent Protein Kinase 1 (CDPK1) by Pyrazolopyrimidine Analogs Decreases Establishment and Reoccurrence of Central Nervous System Disease by *Toxoplasma gondii*

Permalink

<https://escholarship.org/uc/item/4vp5t8v5>

Journal

Journal of Medicinal Chemistry, 60(24)

ISSN

0022-2623

Authors

Rutaganira, Florentine U
Barks, Jennifer
Dhason, Mary Savari
et al.

Publication Date

2017-12-28

DOI

10.1021/acs.jmedchem.7b01192

Peer reviewed



Published in final edited form as:

J Med Chem. 2017 December 28; 60(24): 9976–9989. doi:10.1021/acs.jmedchem.7b01192.

Inhibition of calcium dependent protein kinase 1 (CDPK1) by pyrazolopyrimidine analogs decreases establishment and reoccurrence of central nervous system disease by *Toxoplasma gondii*

Florentine U. Rutaganira¹, Jennifer Barks^{2,a}, Mary Savari Dhason^{2,a}, Qiuling Wang^{2,a}, Michael S. Lopez^{1,b}, Shaojun Long², Joshua B. Radke², Nathaniel G. Jones², Amarendar R. Maddirala³, James W. Janetka³, Majida El Bakkouri⁴, Raymond Hui^{4,5}, Kevan M. Shokat¹, and L. David Sibley^{2,*}

¹Howard Hughes Medical Institute and Department of Cellular and Molecular Pharmacology, University of California, San Francisco, San Francisco, California 94158, USA

²Department of Molecular Microbiology, Washington University School of Medicine, St. Louis, MO, 63130, USA

³Department of Biochemistry and Molecular Biophysics, Washington University School of Medicine, St. Louis, MO, 63130, USA

⁴Structural Genomics Consortium, University of Toronto, MaRS South Tower, 101 College St, Toronto, ON, M5G 1L7, Canada

⁵Toronto General Hospital Research Institute, 200 Elizabeth St., Toronto, ON M5G 2C4, Canada

Abstract

Calcium dependent protein kinase 1 (CDPK1) is an essential enzyme in the opportunistic pathogen *Toxoplasma gondii*. CDPK1 controls multiple processes that are essential to the intracellular replicative cycle of *T. gondii* including secretion of adhesins, motility, invasion, and egress.

*Corresponding Author Information: sibley@wustl.edu, Phone 314-362-8873, ORCID: Oid4lds1.

^acontributed equally, listed alphabetically.

^bAchaogen Inc. 1 Tower Place, #300, South San Francisco, CA 94080

Ancillary Information

Supporting information:

Compound synthesis, characterization, metabolism analysis, x-ray crystallography information, kinome profiling (PDF)

Molecular Formula Strings (CSV)

Compound 24 Homology Model (PDB)

PDB ID Codes: The structure factors and pdb coordinates have been deposited at the protein databank (PDB) with the coordinates 4IHP, 5W8R, 5W80, 5W9E, and 5W91. Authors will release the atomic coordinates and experimental data upon article publication.

Homology models: Compound 24 was modeled using the co-crystal structure of compound 13 (PDB code: 5W9E). Authors will release the atomic coordinates and experimental data upon article publication.

Author contributions: Florentine U. Rutaganira and Michael S. Lopez performed the chemical syntheses and physical characterization of the compounds described here. Jennifer Barks performed the in vitro cell-based assays for parasite and host cell growth inhibition. Mary Savari Dhason and Shaojun Long performed the enzyme purification and enzyme assays. Qiuling Wang conducted the animal studies with assistance from L. David Sibley. Nathaniel Jones and Joshua B. Radke performed the ex vivo tissue cysts experiments. Amarendar R. Maddirala purified select chemicals for in vivo studies. James W. Janetka, provide advice on chemical synthesis. Majida El Bakkouri and Ray Hui performed the structural studies. L. David Sibley and Kevan M. Shokat supervised the research. Florentine U. Rutaganira and L. David Sibley performed data analyses, generated the figures, and wrote the manuscript with input from all authors.

Remarkably, CDPK1 contains a small glycine gatekeeper residue in the ATP binding pocket making it sensitive to ATP-competitive inhibitors with bulky substituents that complement this expanded binding pocket. Here we explored structure-activity relationships of a series of pyrazolopyrimidine inhibitors of CDPK1 with the goals of increasing selectivity over host enzymes, improving anti-parasite potency, and improving metabolic stability. The resulting lead compound **24** exhibits excellent enzyme inhibition and selectivity for CDPK1 and potently inhibited parasite growth in vitro. Compound **24** was also effective at treating acute toxoplasmosis in the mouse, reducing dissemination to the central nervous system, decreasing reactivation of chronic infection in severely immunocompromised mice. These findings provide proof of concept for the development of small molecule inhibitors of CDPK1 for treatment of CNS toxoplasmosis.

Keywords

Parasite; opportunistic pathogen; chronic infection; tissue cyst; bradyzoite; encephalitis; AIDS; protein kinase; ATP-binding pocket; structure activity relationship; pharmacokinetics; X-ray crystal structure

INTRODUCTION

Toxoplasma gondii is a widespread protozoan parasite of animals that causes zoonotic infections in humans. Although most human cases are well controlled, infection in immunocompromised patients leads to serious sequelae, including toxoplasmic encephalitis and pneumonia, which are life-threatening if not treated¹. Although the advent of HAART therapy has reduced the frequency of toxoplasmosis as an opportunistic pathogen in developed countries, it is still a serious complication in many parts of the world where patients do not have adequate access to testing or treatment for HIV infection²⁻⁵. Additionally, toxoplasmosis can cause serious problems in organ transplant and cancer chemotherapy patients due to their immunocompromised status⁶. Furthermore, toxoplasmosis is a recognized cause of severe ocular disease in healthy adults in some locations such as Brazil⁷.

Current therapy for toxoplasmosis is based on combination of pyrimethamine, which blocks dihydrofolate reductase (DHFR), and sulfadiazine, a folate antagonist. Collectively these drugs disrupt replication by inhibiting nucleic acid synthesis. This drug combination is efficacious in treating acute infection through blocking replication of tachyzoites. Unfortunately pyrimethamine is associated with several adverse side effects including anemia due to bone marrow suppression⁸ and many patients experience allergic reactions to sulfonamide drugs⁹. Chronic infections caused by *T. gondii* are typified by slow growing bradyzoites that reside within thick-walled tissue cysts¹⁰. The emergence of bradyzoites upon cyst rupture is thought to give rise to daughter cysts that sustain the chronic infection and contribute to recurrence of actively replicating tachyzoites when the parasite reverts to the lytic form. Hence, treatments that could block re-emergence from the tissue cyst, or block invasion of host cells by bradyzoites could interrupt this cycle and eliminate chronic infection. Unfortunately, current therapies that inhibit DHFR and antagonize the folate pathway are not effective at clearing chronic infection, as evidenced by the high relapse in

immunocompromised patients when therapy is discontinued⁹, presumably due to the slow and sporadic replication of bradyzoites¹¹.

One of the key steps in defining new leads for therapeutic intervention is to identify essential pathways that can be targeted by small molecules. One potential new target is that fulfills these criteria is calcium dependent protein kinase 1 (CDPK1) in *T. gondii*¹². Genetic depletion or chemical inhibition of CDPK1 blocks adhesion secretion and compromises motility, cell invasion, and egress¹², thus demonstrating the essentiality of this target. The X-ray crystal structure of CDPK1 also revealed an unusual feature in the ATP-binding pocket where a glycine (G) residue occupies the gatekeeper position where there is normally a larger hydrophobic residue^{13, 14}. The presence of G gatekeeper is entirely unprecedented in human kinases¹⁵, and CDPK1 is the only kinase in *T. gondii* with this unusual feature¹⁶. As a consequence, CDPK1 is exquisitely sensitive to bulky ATP competitive inhibitors such as pyrazolopyrimidines (PP), which mimic the nucleotide binding interactions with the hinge region within the ATP-binding pocket and project bulky substituents into the expanded hydrophobic pocket created by the G gatekeeper^{17, 18}. These features have been exploited to develop PP analogs that are potent inhibitors of CDPK1 in *T. gondii*^{19–21}, and the most promising of these compounds show good efficacy in mouse models of toxoplasmosis^{22–24}.

Our prior studies involving derivatives with substituents (R1) to the C3 position of the pyrazolopyrimidine (PP) core revealed the importance of the methylene linkage at C3 to confer flexibility of R1 substituent binding²³. However, compounds with the methylene linkage overall were not stable in the presence of rat liver microsomes, potentially due to the methylene bridge being subject to cytochrome P450 metabolism. To address these deficiencies, we have more fully explored the design and synthesis of different heteroatom linkages at the C3 position and expanded the diversity of substituents at the R2 position. Collectively, these rationally driven modifications have identified new TgCDPK1 inhibitors with excellent potency in addition to improved selectivity, metabolic stability, and in vivo efficacy in controlling toxoplasmosis in the mouse.

RESULTS

Design and synthesis of new PP analogs targeting CDPK1

To identify compounds with improved metabolic stability that would also exploit structural differences between CDPK1 and hSrc active sites, we designed and synthesized a compound library containing varied functional groups at R1 attached to the C3 position of the PP core (Scheme 1). These were either linked to the core pyrazolopyrimidine or pyrrolopyrimidine scaffold via methylene or heteroatom linkages (X) in combination with *t*-butyl or various R2 groups at the N1 position (Scheme 1). The hSrc kinase was chosen for initial counter-screening because it contains a threonine (T) gatekeeper residue that represents one of the smallest amino acids found in native human kinases¹⁵. All compounds were synthesized using previously described methods to form the pyrazolopyrimidine scaffold or with advanced pyrrolopyrimidine intermediates^{25, 26}. Methods to generate compounds with methylene linkage at C3 have been previously reported²³ and heteroatom linkages were incorporated using established aryl coupling chemistry^{27–30} (Scheme 1). Detailed

procedures for chemical synthesis and compound characterization are presented in the supplementary information.

Analysis of new PP analogs modified at the R1 position

To develop a structure-activity relationship (SAR) profile, we investigated the effects of modifying the R1 group and different linkers to the core scaffold at position C3 in a series of compounds that contained *tertiary* butyl at the N1 position (Figure 1A). We tested compounds for their potency against CDPK1 in vitro, using an ELISA assay for phosphorylated substrate, described previously²³. In parallel, we tested the inhibitors for their ability to inhibit parasite growth in vitro using a β -Gal expressing line of *T. gondii* to determine EC₅₀ values, as described previously²³. Finally, we screened each analog for stability in vitro in the presence of rat liver microsomes, as a surrogate for estimating in vivo metabolic stability.

Starting with parent compound **1**, replacement of the C3 methylene linker with an ether, thioether, or amine linkage improved metabolic stability for ether and amine linkages (Figure 1A). This result confirms XenoSite in silico predictions of metabolism at the methylene as in compound **1**, that is less likely with ether and amine linkages as in compounds **2 and 4** but is still possible with thioether linkages as in **3** (Supplementary Figure S1)³¹. The thioether linkage was also associated with substantial loss of activity in the parasite inhibition assay (Figure 1A). We also observed increased metabolic stability of the ether linkage over methylene for another compound set consisting of compounds **5, 6**. Analogs bearing halogen substitutions were generally more stable, especially in the presence of the ether linkage. The addition of some *-meta* substituents on the benzyl ring was associated with loss of metabolic stability, despite having an ether linkage, for example addition of the methoxy group in compound **9** and the methyl group for compound **10** (Figure 1A). Since the ether linkage generally improved metabolic stability while maintaining efficacy against parasite replication, we selected ether linkages for further optimization.

Structural interactions between PP compounds and CDPK1

To better understand the binding interactions of PP analogs and the CDPK1 enzyme, we solved a series of high-resolution co-crystal X-ray structures, using previously described methods¹⁴. The co-crystal structure of CDPK1 with the lead compound **1** revealed a characteristic hydrogen-bonding (H-bonding) pattern of interaction between the aminopyridine and the kinase hinge. More specifically, the primary amine at C4 of the PP core acts as a H-bond donor in an interaction with the backbone carbonyl of glutamate (E) 129, and the N5 in the PP core acts as a H-bond acceptor in an interaction with the backbone amide of tyrosine (Y) 131 (Figure 1B). Importantly, the co-crystal structures of compounds **1 – 4** bound to CDPK1 show that these modifications do not substantially change the binding conformations (Figure 1C). Key H-bonding interactions between the PP core and the hinge region are maintained with R1 occupying the hydrophobic pocket formed by the presence of the small G gatekeeper residue (Figure 1C).

Analysis of new PP analogs modified at the R2 position

Previous studies of PP analogs have shown that larger substituents are tolerated at the R2 position and can lead to gain of potency and selectivity for CDPK1²¹. To explore the size tolerance within the CDPK1 pocket at this region, we generated a series of analogs with cyclic amines at R2 (Figure 2A). Structural studies have shown that methyl piperidine in the R2 is positioned to form a H-bond with glutamate (E) 135 in the ribose binding region of the ATP pocket of CDPK1^{19, 20}. A co-crystal structure of compound **13** confirmed this interaction is also present in the series studied here (Figure 2B). The piperidine is predicted to be protonated under physiological conditions and as shown in the co-crystal structure, the additional H likely forms a salt bridge with glutamine (E) 135 (Figure 2B). We explored a series of cyclic amines based on piperidine where we elucidated the importance of proper placement and direction of the amine to form the favorable charge-charge salt bridge interaction with E135. We found that any deviation from the piperidine of **13** in this series abrogated CDPK1 activity and decreased inhibition of parasite replication in culture (Figure 2A). Compounds **16** and **15**, which contain a tetrahydropyran and pyridine group, respectively, each significantly lost potency, emphasizing the key contribution of the H-bond donor of the piperidine (Figure 2A). On the other hand, all cyclic amines showed greatly enhanced stability in the rat liver microsome assay thus providing much support for further R2 modification as an approach to improving metabolic stability (Figure 2A).

In another series, we explored the combination of methyl piperidine at R2 together with the prior functional groups at R1 (Figure 3A). Consistent with findings above, the methyl piperidine containing analogs generally showed improved metabolic stability in comparison to their *t*-butyl counterparts (Figure 1A, 3A). For example, the presence of the methyl piperidine in compound **17** could impart stability despite having a methylene linkage to C3 of the PP core (Figure 3A). Compounds with additional halogens in the benzyl ring at R1 gained further increases in microsome stability (e.g. **21** and **22**) (Figure 3A). Furthermore, there were no significant differences between pyrazolopyrimidine and pyrrolopyrimidine as the core scaffold as demonstrated by compounds **18** vs. **23** (Figure 3A).

Despite the reproducible ability of methyl piperidine to improve microsome stability throughout the entire series, this modification also resulted in reduced biochemical potency and ability to block parasite replication. Hence, incorporation of methyl piperidine at R2 results in a tradeoff between improved metabolic stability and loss in potency. This effect may be explained by the larger size of these inhibitors that may not be as easily accommodated in the CDPK binding pocket. The combination of ether linked R1 as *m*-Cl with R2 piperidine as in compound **13** showed the largest improvement over parent compound **1** while retaining reasonable activity in both inhibition CDPK1 and parasite growth (Figure 3A). In contrast, methylation of the piperidine nitrogen in compound **25** led to a loss in potency, further highlighting the importance of the H-bonding ability of the protonated amine (Figure 3A). Converting the piperidine to a 6-membered ring δ -lactam in compound **26** also led to a loss in enzyme potency and a complete loss in anti-parasitic activity (Figure 3A). We also explored modifying the piperidine by addition of di-fluorine (di-F) *-meta* to the amine, as such modifications are known to favorably affect the properties of drug-like molecules³². The di-F modification in compound **24** vs. **13**, which both have

ether-linked R1 substitutions to the PP core, slightly improved enzyme inhibition and anti-parasitic activity (Figure 3A). A homology model of **24**, based on the co-crystal structure of compound **13** with CDPK1, suggests that the piperidine amine is still in an appropriate position to interact with E135 (Figure 3B, Table 1). We also made a similar modification of di-F in a *-meta* position to the piperidine amine in compound **18** to generate the compound **28**, both of which have a thioether linkage connecting R1 to C3 in the PP core. Surprisingly in this case, the di-F modification reduced enzyme activity and greatly diminished anti-parasitic activity. Modification of R2 to contain a trifluoromethylcyclopropyl moiety was also synthesized in an attempt to reduce metabolic instability, based on a previous study showing this modification can improve stability of biaryl compounds relative to those containing *t*-butyl³³. This compound **27** lost potency (Figure 3), suggesting it does not optimally fit in the CDPK1 ATP binding pocket, moreover it did not improve stability, perhaps due to the methylene linkage of the trifluoromethylcyclopropyl moiety to N1 of the core.

Inhibition of CDPK1 in vitro correlates with parasite growth inhibition

To compare the potency of all of the new PP analogs synthesized here, we plotted the log₁₀ values for CDPK1 enzyme inhibition (IC₅₀) vs. log₁₀ values for parasite growth inhibition (EC₅₀) (Figure 4A). Fitting these data with a linear regression analysis indicated a reasonable correlation ($r^2 = 0.58$), supporting the conclusion that the activity of these compounds against parasite growth stems largely from inhibition of CDPK1. However, the fact that this correlation is not higher suggests that *in vivo* potency is also affected by other factors including differences in cell permeability. Some inhibitors lie above the diagonal line, which represents a perfect correlation, indicating they are less potent in blocking parasite growth, perhaps due to differences in cell permeability or efflux (Figure 4A). Among the most potent inhibitors was the initial lead **1**, and derivatives that contain an oxygen linkage at R1 (e.g. **2** and **10**), as well as those that contain the methyl-piperidine at R2 (e.g. **13**, **24**) (Figure 4A). Based on a combination of potency, selectivity and PK properties, we prioritized compounds and selected these five analogs for further study. Other compounds that were potent in both assays were deprioritized for lack of specificity (e.g. **4**) or lack of stability (e.g. **9**).

Metabolic stability and cellular uptake of PP analogs

To help choose PP analogs most likely to be active in vivo, we broadly examined the physical properties, metabolic stability in mouse liver microsomes, and cellular uptake of a select group of PP analogs (Table 1). All compounds have modest cLogP values, consistent with their intermediate hydrophobicity, and are predicted to have relatively small total polar surface area, properties that should facilitate penetration of the CNS (Table 1). Consistent with the findings in rat liver microsomes, the ether linkage in compound **2** reduced metabolic clearance in mouse liver microsomes when compared to compound **1**, although both values are still relatively high (Table 1). Compound **10**, which had similar clearance to compound **1** in rat liver microsomes despite having an ether linkage, was more rapidly cleared in mouse liver microsomes (Table 1), suggesting the methyl group at C3 might be prone to metabolism. Stability was further improved when the R2 group was switched from *t*-butyl to methyl piperidine as in compounds **13** and **18**. However these latter two

compounds, which contain a basic amine group that is charged a neutral pH, were also associated with substantial efflux in MDCK cells (Table 1). In addition to the many other useful aspects of fluorine substitutions in medicinal chemistry, in some contexts it has been shown to reduce the basicity of proximal amines by lowering the pKa³⁴. Accordingly, we modified the piperidine ring by addition of di-fluorine (di-F), a modification reduced the pKa and nicely eliminated the efflux problem (**24** and **28**; Table 1). However, metabolic stability was diminished by the di-F modification in these compounds. Analogs such as **1** showed high levels of plasma protein binding (PPB) (i.e. 99%), however this property was greatly reduced for compounds containing methyl piperidine or the di-F methyl piperidine (Table 1). Importantly, none of the PP analogs tested affected the growth of human foreskin fibroblasts (HFF) cells in vitro at 10 μ M, indicating that they are not toxic to host cells (Table 1).

Analysis of target specificity of select PP analogs

To provide an assay for inhibitor selectivity we cloned a variant of human Src, which has a threonine (T) residue at the gatekeeper (c-Src allele), which provides for an intermediate level of sensitivity to pyrazolopyrimidine compounds¹⁸. Although the initial lead compound **1** potently inhibited hSrc, modification of the R1 linkage to the PP core via an ether or thioether at C3 led to greater selectivity (Figure 1A). Modification of R2 to include cyclic amines, including piperidine, also led to large increases in selectivity for CDPK1 over hSrc (Figure 2A). Although Src has been used as a surrogate for human kinases with intermediate sensitivity to PP analogs^{19, 21}, it is only one member of a diverse family of tyrosine kinases that differ substantially in their sensitivity to PP inhibitors³⁵. As such, we profiled select inhibitors **1**, **2**, **13**, and **24**, which marked key transitions in our SAR profile. We screened all four analogs at 1 μ M against a broad panel of 489 wild type and disease-associated human kinases (Figure 5). Inhibitor selectivity increased along our SAR profile, starting from thirty-nine kinases that are inhibited or displaced by compound **1** by over 50% to only one kinase (CK1 ϵ) that was inhibited or displaced by **24** by over 50% (Figure 5, Supplementary Table S2). Although compounds **13** and **24** exhibited IC₅₀ values of 100 nM at 2 μ M ATP, these values were increased almost 10 fold in the presence of 100 μ M ATP (Supplementary Table S2). Additionally, we profiled an earlier inhibitor 3-methyl-benzyl-PP (compound **1** in²³) to compare our initial lead **1** in this prior series. We determined that the selectivity profile for both of these compounds was similar (Supplementary Figure S3), while selectivity was greatly increased for compounds **13** and **14**. Full inhibitor profiling data is provided in the supplementary information (Supplementary Tables S3–S5).

Potency of select PP analogs against ex vivo bradyzoites

Previous studies have emphasized the ability of PP analogs to block host cell invasion and egress by the rapidly growing tachyzoite stage of *T. gondii*^{19, 21, 23}. To examine the ability of our PP inhibitors to block invasion of bradyzoites, we purified mature tissue cysts from the brains of chronically infected mice and treated them in vitro with selected PP inhibitors. We compared the effects of treatment for short intervals (i.e. 4 hr followed by wash-out and further culture in the absence of compound) vs. continuous treatment during a 10–14 day plaquing assay. Consistent with previous reports showing that treatment with pyrimethamine requires overnight treatment to be effective in blocking tachyzoite growth³⁶ we observed

that short-term treatment with pyrimethamine had minimal effect on infection by bradyzoites while continuous treatment blocked plaque formation (Figure 4B). In contrast, the PP inhibitors showed good (e.g. **13**), or excellent (e.g. **1**, **24**), ability to block infection following even short-term incubation (Figure 4B). Because the compounds were only present during the initial interaction of the parasite with the host cell monolayer, we interpret these results to indicate that PP inhibitors can block bradyzoite entry into host cells during the 4 hr treatment period, resulting in greatly diminished plaque formation. Additionally, continual culture with PP compounds resulted in greater inhibition (Figure 4B), consistent with its ability to block the multiple rounds of invasion and egress that occur during plaque formation, although it is likely that tachyzoites predominate during these longer-term assays.

Mouse pharmacokinetic studies

We examined the pharmacokinetics (PK) of several PP inhibitors in mice following either i.v. injection or p.o. administration in mice. Compounds **1** and **2** showed reasonable oral bioavailability (F) ranging from ~25–30%, C_{max} levels, and moderate clearance (Cl) values that were below the level of single pass circulation through the liver in mouse (~90 ml/min/kg) (Table 2). Compound **10** showed a higher clearance rate, but had similar half-life (T_{1/2}) to **1** and **2** of ~1.5 to 2 hr (Table 2). However, this compound suffered from poor oral bioavailability (Table 2). Although compound **13** had greater in vitro stability in microsomes (Table 1), it also displayed rapid clearance in vivo, perhaps due to efflux as indicated above. Compound **13** also showed lower C_{max} values and high tissue exposure as evidenced by its volume of distribution (V_{ss}) (Table 2). Finally, compound **24** showed the best combination of properties with good C_{Max} following oral dosing, moderate clearance rate, T_{1/2} ~1.5 hr, and very high oral availability (e.g. ~94%) (Table 2). These collective properties of compound **24** provided the best PK profile and highest values for AUC, reflecting prolonged serum exposure following oral dosing.

Based on these favorable properties, we examined the PK of **24** in mice using increasing oral doses from 10, 25, and 50 mg/kg (Figure 4C). At higher doses, **24** showed a two-phase decay curve in plasma, with rapid initial drop followed by a more gradual plateau that was seen at 25 and 50 mg/kg (Figure 4C). Based on its protein binding properties (12% free in serum), the concentration of compound **24** in serum would need to be 2.08 μM, for the free value to attain a level equivalent to the in vitro EC₅₀ of ~0.250 μM. This corresponds to a value of 856 ng/ml in serum, as shown by the red line in Figure 4C. The protein bound fraction in brain was slightly higher at 97.2%, or 2.8% free, and the ratio of total compound in the CNS vs. serum was 5.6, for an effective brain vs. plasma ratio ~1.3. Consequently, we would expect that the brain free concentration of compound **24** in the brain was approximately the same or slightly higher than that shown for serum in Figure 4C.

Treatment of acute toxoplasmosis

Based on its favorable PK parameters, we tested compound **24** for its ability to prevent toxoplasmosis in the mouse model. Following an initial loading dose of 50 mg/kg, **24** was administered orally at 25 mg/kg BID for 6 days, beginning 24 hr after challenge with tachyzoites of the ME49 strain of *T. gondii*. Treatment with **24** decreased the frequency of lethal infection (Figure 6A), and this was associated with reduced weight loss (Figure 6B)

and with decreased tissue burdens of the parasite, as revealed by bioluminescent imaging (Figure 6C). Consistent with a decrease in acute burden, there were fewer tissue cysts formed in the brains of chronically infected mice following treatment with **24** (Figure 6D). The dramatic ability of **24** to decrease dissemination was further shown by bioluminescent imaging, where control animals showed extensive expansion of the parasite within the peritoneum at day 8 and spread to the head at day 18 (Figure 6E,F). In contrast, treated mice were able to restrict the growth of the parasite to the site of injection and did not show detectable signal in the head (Figure 6E,F). Following treatment with **24**, many animals showed tissue cyst levels below the levels of detection (40 cysts per brain) (Figure 6D). These animals were subsequently bio-assayed by oral feeding of 20% of their brain homogenate into a naïve interferon gamma receptor knock out mouse (*Ifngr1*^{-/-}). Although 5 of 6 recipient animals succumbed to infection, reflecting a low level of chronic infection in the donor, one remained alive, indicating that compound **24** treatment had resulted in a complete cure in this animal (Figure 6D, red triangle).

Treatment of reactivated CNS toxoplasmosis

To determine whether compound **24** could prevent reactivation of chronic toxoplasmosis, we utilized mice lacking the IFN γ receptor (i.e. *Ifngr1*^{-/-}), which are highly susceptible and rapidly succumb to infection³⁷. Treatment of such animals with sulfadiazine will suppress the growth of tachyzoites, while allowing the development of chronic tissue cysts³⁸. Subsequent removal of sulfadiazine results in rapid reactivation, characterized by CNS encephalitis, pneumonia and death³⁸. We injected *Ifngr1*^{-/-} mice with a type II strain capable of causing chronic infection and treated them from day 2–22 with sulfadiazine in the drinking water, which prevented otherwise lethal infection. Following removal of sulfadiazine (48 hr later), mice were treated with compound **24** at a dose of 25 mg/kg or 40 mg/kg BID, or with vehicle only control, by oral gavage for 8 days (Figure 7A). Withdrawal of sulfadiazine from the control animals led to rapid reactivation of chronic infection led to death of the control mice within 10 days (Figure 7B). In contrast, treatment with compound **24** prolonged survival (Figure 7B). We also monitored the progression of infection using bioluminescence. At the beginning of the treatment period, all of the animals were negative for bioluminescence, consistent with the infection being chronic. Monitoring of the control animals revealed that reactivation was first centered in the CNS, with later spread to the lungs prior to death (Figure 7C). In contrast to the rapid expansion of parasites seen in control mice, the bioluminescence signal was muted in compound **24** treated mice, and reactivation was significantly delayed (Figure 7C). Consistent with this delay in reactivation, compound **24** treated mice survived significantly longer (Figure 7B). One animal treated with compound **24** at 25 mg/kg and two animals treated at 40 mg/kg remained negative for bioluminescence signals and survived for an additional 22 days after removal of compound **24** (red triangles in Figure 7B). Subsequent bioassay of brain homogenates from these treated mice into naïve *Ifngr1*^{-/-} mice did not result in transfer of infection, confirming that these animals had been cured (Figure 7B).

DISCUSSION

In previous work, we demonstrated that PP inhibitors containing *meta* chloro benzyl substituents at C3 of the PP core provide potent inhibition of CDPK1 in *T gondii*³⁶. However, when coupled with isopropyl or *t*-butyl at R2, these compounds suffer from metabolic instability³⁶. Our profiling of host kinases here also reveals that compounds like **1** lack specificity, and this is also likely true of other related derivatives that share this basic architecture. To alleviate this problem, we altered the linkage connecting R1 to C3 from a methylene to a heteroatom consisting of O, S, or N. An ether linkage proved most optimal in increasing stability and selectivity, while compounds with a thioether linkage were typically less active and compounds with an amine linkage were less selective. The reasons for these differences are not exactly clear as co-crystal structures of these analogs showed very close overlap of the analogs in the binding pocket. The lower activity of the thioether linkage may relate to the bulkier nature of this atom within the linker, which is very close to the hinge region in the crystal structure. We have previously shown that even subtle modification to this linker, such as substitution of fluorine for hydrogen, ablates activity²³.

By combining the ether linkage at C3 with a methyl piperidine at R2, we achieved further gains in specificity, with only modest loss of potency. Other modifications to R2, such as including a pyridine or methylation of the piperidine nitrogen, ablated activity suggesting that the unsubstituted alkyl amine is critical for the potency. Indeed a co-crystal structure of compound **13** revealed this amine is important for forming a hydrogen bond with glutamate (E) 135 in the ribose-binding region, likely stabilizing the interaction of the compound with the ATP-binding pocket. Addition of the piperidine group in the scaffold described here also resulted in dramatic improvement in specificity over host kinases compared to the initial lead compounds **1** and **2**. Compounds **13** and **24** only potently inhibited a single human kinase CK1 ϵ under conditions tested here. Surprisingly, CK1 ϵ is also sensitive to other PP analogs including 1-NM-PP1 and 1-NA-PP1, despite its methionine (M) gatekeeper, which is normally a hallmark for resistance to such analogs³⁹. The sensitivity of CK ϵ to PP analogs has been attributed to an unusual flexibility in the M side-chain that allows access of bulky PP analogs into the ATP-binding pocket⁴⁰. Further modification of the PP scaffold may result in inhibitors that would retain potency for CDPK1 over CK ϵ . However, this off target activity may be less of an issue in vivo since compound **24** retains good potency against parasite growth in a cell-based assay, while off target activity against CK ϵ drops appreciably at higher ATP levels.

Despite the improvements in specificity achieved with the piperidine analogs, these charged primary amines suffered from efflux problems in our study, likely due to the high pKa³⁴. Addition of di-F in the piperidine ring decreased the predicted pKa and eliminated the efflux problem, consistent with previous examples in other scaffolds³⁴. Previous experimental measurements of piperidine amines with fluoro substituents³⁴, combined with computational predictions of the compound **24** piperidine amine pKa suggest that the piperidine amine in compound **24** is partially protonated at physiological pH. Based on these properties and its potency, we would predict that compound **24** is still able to form a H-bond with E135 in CDPK1. Unfortunately, modification of di-F *meta* to the amine in the piperidine was also associated with some loss of metabolic stability, which likely limited its in vivo efficacy. We

did not explore modification with fluorine-directed modifications at other positions in the piperidine ring, but conceivably some of these may have a more optimal combination of features.

One of the goals of our study was to obtain molecules with better metabolic stability to improve in vivo PK properties for treating acute and chronic toxoplasmosis in the mouse. Compound **24** exhibited many of the desired properties in terms of PK in the mouse. Although C_{max} levels were high, it was relatively rapidly cleared from serum, likely as a consequence of metabolism in the liver as the half-life in microsomes was relatively short. This was partially offset by high oral availability and moderate protein binding, resulting in reasonable serum profiles and good AUC profiles. However, we were only able to obtain free serum levels that exceeded the EC₅₀ based on free drug for a period of ~ 2 hr after oral dosing in the mouse. Nonetheless, dosing schemes of 25–50 mg/kg were able to decrease acute infection, preventing weight loss and death in a majority of immunocompetent animals. Additionally, treatment during acute infection resulted in dramatically lower cyst counts during chronic infection, likely as a consequence of decreasing dissemination to the CNS. Indeed, treatment was sufficient to provide a complete cure in one animal with no evidence of chronic infection.

Although previous studies have largely focused on the acute infection model, the primary concern for immunocompromised patients is the reactivation of prior chronic infections⁹. Here we modeled this situation using severely immunocompromised *Ifngr*^{-/-} mice, which are highly susceptible to *T. gondii* infection³⁷. As *Ifngr*^{-/-} mice completely lack the ability to respond to IFN γ , a critical mediator of host defense, it is likely that a single tissue cyst, or single viable organism, is capable of causing lethal infection in this model. Hence they provide an extremely sensitive measure of the ability of compounds to cure infection. Treatment with atovaquone³⁸ or artemisinin⁴¹ derivatives is able to prolong survival of such severely immunocompromised mice, but treated animals ultimately always succumb to infection following removal of these drugs. Similarly, treatment with sulfadiazine is only able to prevent lethal infection in this model, but not eliminate the tissue cysts, such that when it is removed, animals quickly succumb due to reactivation of rapidly growing tachyzoites. Treatment with compound **24** prolonged survival of *Ifngr*^{-/-} mice and resulted in a radical cure in some animals, a result not previously seen with other compounds. The efficacy of compound **24** in this model likely stems from its ability to block tachyzoite invasion and egress, but it was also able to block bradyzoite invasion in vitro, suggesting it may directly affect the formation and turnover of cysts in vivo. Other PP analogs have been reported to reduce the chronic cyst burden in infected mice, albeit at very high serum doses, which exceed the level where they are selective for CDPK1¹⁹. In contrast, compound **24** retains anti-toxoplasma activity at very modest serum levels, which are well within the range where it is selective for CPDK1 in *T. gondii*^{12, 23}.

CONCLUSIONS

CDPK is an essential kinase in *T. gondii* and hence has been the focus of development of potent and selective inhibitors. Here we report new PP inhibitors that were designed to improve metabolic stability and specificity for CDPK1. The optimal molecule in this series

compound **24** showed low nanomolar inhibition of CDPK1 in vitro, submicromolar inhibition of parasite growth in vitro, and improved metabolic stability. In vivo administration of this analog, which showed excellent oral availability and moderate PK parameters, decreased the severity of acute infection, reduce tissue cyst levels, and delay reactivation of chronic toxoplasmosis in the mouse. Additionally, compound **24** is remarkable in being able to completely cure a portion of immunocompromised animals. As radical cure is currently not possible for humans infected with *T. gondii*, compounds that can achieve this goal with higher efficacy would greatly enhance the potential utility of PP analogs for treatment of toxoplasmosis. Collectively, these advances underscore the utility of the PP scaffold as a new therapeutic agent for treatment of acute and chronic toxoplasmosis.

EXPERIMENTAL SECTION

Chemical synthesis

Starting materials, solvents and reagents obtained commercially were reagent grade and were used without further purification. NMR spectra were obtained at the University of California, San Francisco NMR facility: ¹H NMR were recorded on a Bruker AvanceIII HD 400 at 400 MHz and ¹³C spectra were recorded on a Bruker AvanceIII HD 400 at 400 MHz or a Bruker Advance DRX500. High-resolution mass spectra (HRMS) were acquired by electrospray ionization (ESI) in positive ion mode using Finnigan LTQ FT mass spectrometer (Thermo) at the QB3/Chemistry Mass Spectrometry Facility (University of California, Berkeley). Samples were directly injected into ESI source via syringe pump with flow rate 5 uL/min. Reactions were monitored by thin layer chromatography (TLC), using Merck silica gel 60 F254 glass plates (0.25 mm thick). Flash chromatography was conducted with Teledyne Isco RediSep Rf silica flash cartridges on a Teledyne Isco CombiFlash Rf+. All RP-HPLC were performed with a Waters 2545 binary gradient module equipped with an XBridge prep C18 column using H₂O + 0.1% formic acid and CH₃CN + 0.1% formic acid (5–95% gradient) while monitoring at 254 nm. All final compounds were >95% pure as measured by Liquid Chromatography Mass Spectrometry (LCMS) using a Waters Acquity UPLC/ESI-TQD BEH C18 (1.7 μm) column using H₂O + 0.1% formic acid and CH₃CN + 0.1% formic acid (5–95% gradient) over 1.8 min at 600 μL/min. Full compound characterization details are presented in the supporting information. All compounds reported here were screened for Pan Assay Interference (PAINS) and found to pass all the filters based contained in the FAF-Drugs4 web-server (<http://fafdrugs4.mti.univ-paris-diderot.fr/>).

Parasite strains and cell lines

Tachyzoites of *T. gondii* strains were grown in monolayers of human foreskin fibroblasts (HFF) maintained in complete medium (DMEM containing 10% FBS, 10 mM glutamine, and 10 μg/ml gentamycin) at 37°C in 5% CO₂. Following natural egress, tachyzoites were purified in HBSS containing 10 mM HEPES, 0.1 mM EGTA and separated from host debris using 3.0 micro polycarbonate membrane filters, followed by centrifugation at 400g. HFF monolayers obtained from an anonymous donor were provided by Dr. John Boothroyd's laboratory (Stanford University). All strains and host cell lines were determined to be mycoplasma negative using the e-Myco plus kit (Intron Biotechnology).

Enzyme expression and purification

Full-length *T. gondii* CDPK1 enzyme was expressed with a C-terminal His tag in pET22b(+), as described previously¹². CDPK1 was expressed in BL21 (DE3)V2RpAcYc-LIC+LamP E coli, which contains the LamP phosphatase. A cDNA fragment encoding human Src (hSrc) kinase domain ranging from amino acids 254–536 amino acids was amplified using the primers Scr-F (GATATACATATGCAGACTCAGGGCCTGGC) and Scr-R (GTGGTGCTCGAGGAGGTTCTCCCC), and cloned into pET22b using restriction enzymes NdeI and XhoI. hSrc containing a Thr gatekeeper residue (equivalent of Thr338 in the full length sequence of the c-Src allele) was expressed in BL21 (DE3)V2RpAcYc-LIC+LamP E coli, which contains the LamP phosphatase. Following overnight growth in Terrific Broth at 37°C, the culture was diluted 1:100 and grown for 3 hr at 37°C (O.D. 0.6–0.8), then induced with 0.3 mM IPTG during overnight growth at 15°C or 30°C. Cells were lysed by sonication and soluble proteins purified using HIS-select Nickel Affinity Gel. Purified proteins were dialyzed (50 mM Tris-HCL, pH7.5, 150 mM NaCl), and stored in 25% glycerol containing 0.5 mM DTT at –80°C. Protein purity and concentrations were determined by SDS-PAGE and staining with SYPRO Ruby (Invitrogen).

Crystallography method

For the purpose of crystallization, recombinant *Tg*CDPK1 was expressed, purified, and set up in crystal trial with inhibitors as previously described¹⁴. Diffracting crystals were obtained by co-crystallization with compounds **3** (PDB code: 5W9E), **1** (PDB code: 5W8R), **2** (PDB code: 41H8), **13** (PDB code: 5W80), and **4** (PDB code: 5W91). Crystallographic data were collected at beam line 19ID of Argonne National Laboratory's Advanced Photon Source (<http://www.sbc.anl.gov/index.html>) and processed using *HKL-3000*⁴². All structures were solved using Phaser for molecular replacement and the previously deposited *Tg*CDPK1 coordinates (PDB code: 41H8) as a search model. The models were refined using *Buster*⁴³ and *REFMAC*⁴⁴ combined with iterative manual model building using the molecular graphics program *Coot*⁴⁵. The geometry of all final models was checked using *MolProbity*⁴⁶. Crystallographic details and refinement statistics are summarized in Table S1. Atomic coordinates and experimental data will be released on publication.

Homology modeling

Compound **24** was modeled using the co-crystal structure of compound **13** (PDB code: 5W9E) in Molecular Operating Environment (MOE) version 2015.1 by Chemical Computing Group⁴⁷. Di-Fluorine was added to the piperidine of compound **13** using the ligand builder to create compound **24** and the structure was prepared and minimized using LigX with the Amber10:EHT force field (used Protonate3D for protonation, allowed ASN/GLN/HIS “Flips” in Protonate3D, deleted water molecules farther than 4.5Å from compound **24** or CDPK1, tethering parameters: receptor strength at 5000 to minimize large changes to the CDPK1 backbone, fixed atoms father than 8Å away from compound **24**, hydrogens close to compound **24** not fixed, and refined compound **24**-CDPK complex to an RMS gradient of 0.1kcal/mol/Å).

Enzyme assays and IC₅₀s

CDPK1 activity was monitored based on phosphorylation of syntide-2 peptide (Callbiochem) that was detected using mAb MS-6E6 (MBL Intl, Corp) using an ELISA protocol described previously²³. Kinase reactions were conducted at 30°C for 20 min in 20 mM HEPES, pH 7.5, 10 mM MgCl₂, 1 mM DTT, 2.5 mM CaCl₂, 0.1 mM EGTA, 0.005% Tween 20. Reactions were conducted using 25 μM ATP (the K_m for the enzyme) using 140 ng of kinase per reaction. To determine the potency of inhibitors, duplicate wells were treated with a range of compound concentrations from 10 μM to 0.5 nM. Inhibitors were pre-incubated with the enzyme in the reaction buffer for 10 min before addition of ATP. Individual IC₅₀ values were determined from two or more independent biological replicates and are reported as mean values. Src activity was monitored by phosphorylation of the Abltide peptide (EAIYAAPFAKKK, Enzo Life Sciences) that was detected using a monoclonal antibody to phosphotyrosine (Sigma) using an ELISA protocol similar to that used for CDPK1 above. Kinase reactions were conducted in 50 mM Tris-HCl, pH 7.5, 10 mM MgCl₂, 2.5 mM MnCl₂, 0.2 mM DTT, 0.5 mM EGTA. Reactions were conducted using 5 μM ATP (the K_m for the enzyme) using 75 ng of kinase per reaction. Compounds were tested at 10 μM in duplicate, in two biological replicates, and values are reported as mean ± S.D. For compounds that showed > 50% inhibition at 10 μM, serial dilutions from 10 μM to 0.5 nM were tested in duplicate to derive IC₅₀ values.

CK1ε (ThermoFisher) activity was monitored based on phosphorylation of dephosphorylated casein (Sigma-Aldrich) under the following conditions: 50mM TRIS (pH 7.4), 10mM MgCl₂, 0.4 mg/mL casein, 2.5 mM DTT, 2% DMSO, 0.1 mg/mL BSA, 2 μM ATP (K_{m_{app}}), 1μCi 32P-ATP (Perkin Elmer), 5 nM CK1ε. Additional activity assays were done at 100 μM ATP with 10nM kinase. To determine the potency of inhibitors, duplicate wells were treated with a 10-fold dilution of compound from 200 μM to 200 pM. Inhibitors were pre-incubated with the enzyme in the reaction buffer for 15 min before addition of ATP and 32P-ATP. Upon completion of the reaction (10 minutes for K_{m_{app}}, 55 minutes for 100 μM ATP) 3μL was spotted onto P81 paper. The paper was dried for 5 minutes under a heat lamp followed by 1×30second wash and 6×5min washes in 1% Phosphoric Acid. The paper was dried for 15 minutes under a heat lamp followed by overnight exposure to a phosphor screen imaged on a Typhoon 9500. Intensities were quantified using densitometry and IC₅₀ values were determined from quantification of two independent biological replicates of triplicate dose response determined by fitting the data to a sigmoid function in Prism 7.0 (GraphPad Software) and are reported as mean values.

Kinome screen

Human kinome profiling was conducted using the ThermoFisher Scientific SelectScreen ACCESS program to profile 489 kinases utilizing three assay formats: Z'-LYTE (284 kinases), Adapta (39 kinases), and LanthaScreen (166 kinases). Z'-LYTE and Adapta yield % inhibition values based on the mean of 2 points that measure the ability of the compound to inhibit an active kinase. LanthaScreen yields % displacement values based on the mean of 2 points that measure the ability of the inhibitor to displace a tracer bound to an inactive or weakly active kinase. Inhibitors were screened at 1 μM.

Parasite growth assays and EC₅₀s

Parasite growth inhibition assays were conducted using the type I RH strain, 2F clone that expresses bacterial β -galactosidase (β -gal), as described previously²³. Compounds dissolved in DMSO at 10 mM stocks were diluted in medium to two times final concentrations and added to an equal volume of medium containing 5×10^2 parasites and incubated for 20 min. Mixtures of compounds (ranging from 10 μ M to 0.01 nM) containing 0.1% (v/v) DMSO, or DMSO alone were added to monolayers of HFF cells grown in 96 well plates, centrifuged at 300 *g* for 5 min, and returned to culture at 37°C, 5% CO₂. After 4 hr, the plates were washed to remove extracellular parasites and compounds, and then returned to culture for 72 hr. At the end of the incubation period, the monolayer was lysed in 1% Triton X-100 and β -gal activity monitored using 1 mM chlorophenol red- β -D-galactopyranoside by absorption at 570 nm, as described previously²³. Individual EC₅₀ values were determined from three or more independent biological replicates and are reported as mean values.

Host toxicity assays

HFF cells were plated in complete medium and allowed to adhere for 4 hr at 37°C, 5% CO₂. Compounds diluted to 10 μ M in 0.1% (v/v) DMSO, or DMSO alone, were then added and cells were incubated for an additional 72 hr. Following the incubation period, samples were evaluated using a cell proliferation assay (CellTiter 96 Aqueous Non-Radioactive Cell Proliferation Assay, Promega Corporation). As a positive control, mitomycin C (10 μ M) was included in each plate. Compounds were tested in duplicate, in two biological replicates, and values are reported as means \pm S.D.

In vitro analysis of uptake, efflux, metabolism, and protein binding—Assays to monitor uptake and efflux of compounds by polarized epithelial cells were conducted by Absorption Systems Inc. (Exton, PA, USA). In brief, Caco-2 cells (Clone C2BBel from ATCC) were grown to confluence on collagen-coated polycarbonate membranes on transwell plates. Permeability assays were conducted in Hank's balanced salt solution, containing 10 mM HEPES, 10 mM glucose, pH 7.4. Compounds were added at 5 μ M to the apical (A) vs. basolateral (B) side and duplicate samples taken at 120 min. Samples were analyzed by LC-MS/MS and expressed as apparent permeability (P_{app}) for uptake (A to B) vs. efflux (B to A) and efflux ratio (P_{app} (B to A) / P_{app} (A to B)).

The stability of compounds in the presence of rat or mouse liver microsomes was conducted by Absorption Systems, Inc. In brief, rat liver microsomes, or mouse rat liver microsome were incubated with compounds at 1 μ M in a shaking water bath for 60 min. Aliquots were withdrawn at intervals, extracted, and analyzed by LC-MS/MS to evaluate the remaining parent compound. Half-lives were calculated using a single-phase exponential decay equation (Graph Pad). Intrinsic clearance was calculated as $CL_{int} = k/P$, where k is the elimination rate constant and P is the protein concentration in the assay. For plasma protein binding, compounds were incubated at 5 μ M in CD-1 mouse plasma and protein bound fractions were monitored by equilibrium dialysis.

In vivo pharmacokinetic studies—Pharmacokinetic (PK) studies were conducted by Sai Life Sciences Limited (India). Compounds were administered orally in 50% PEG-400 in

PBS, while for i.v. administration, compounds were dissolved in 20% PEG-400 -PBS. Mean plasma concentrations were determined following a single i.v. dose of 3 mg / kg in male Swiss Albino mice by sampling at 0.05, 0.25, 1, 2, 4 and 8 hrs. Separately, male mice were used for monitoring mean plasma concentrations following single oral dose 10 /mg / kg with similar time points. Separate animals were used to determine the brain distribution relative to plasma levels at 1 hr following a single oral dose of 10 mg/ kg. Selected compounds were tested for dose response of plasma concentrations following single or multiple oral administration of a single dose of 10, 25, and 50 mg/ kg at time intervals of 0.25, 1, 2, 4, 8 and 24 hr. Plasma samples were separated processed by precipitation in acetonitrile and analyzed by LC-MS/MS. Pharmacokinetic parameters, including those for plasma versus brain, and oral bioavailability, were calculated with the non-compartmental analysis tools of the Phoenix WinNonLin (v6.3).

Animal Studies—Animals were obtained from Jackson Laboratories and housed at Washington University in accordance with the U.S.A. Public Health Service Policy on Humane Care and Use of Laboratory Animals. Animals were maintained in an Association for Assessment and Accreditation of Laboratory Animal Care approved facilities and were approved by the Institutional Animal Studies Committee at the School of Medicine, Washington University in St. Louis.

Ex vivo bradyzoite treatment assays

Adult (8–12 weeks old) female CD1 mice were infected with tachyzoites of the Pru *hxg ku80*; LDH2-GFP (PRU-GFP)⁴⁸ or ME49 *hx::FLUC*⁴⁹ strains expressing firefly luciferase (FLUC)⁴⁹ and allowed to develop chronic infections. Adult (8–12 weeks old) CBA/J mice were orally infected with 10–20 tissue cysts of the ME49 *hx::FLUC* strain. At 3–6 weeks post-inoculum, brains were isolated from 2–3 animals and tissue cysts purified from brain homogenate by Percoll gradient, as previously described¹¹. A serological pipette was used to isolate the ~9.0 mL of gradient between the erythrocyte layer and the brain homogenate layer after the initial centrifugation step (1,200g for 15 min at 4°C). Following purification, cysts were resuspended in acid-pepsin solution (170 mM NaCl, 60 mM HCl, 0.1 mg/mL pepsin (1:10,000 activity)), incubated for 10 min at 37°C and then neutralized by addition of sodium carbonate solution (94 mM). Liberated bradyzoites were inoculated into parallel 6-well plates containing HFF monolayers with compounds (constant treatment vs. washout). At 4 hr post-infection, the washout 6-well plate was rinsed 3 times in fresh media to remove cell debris and non-invaded parasite and returned to incubator with fresh culture medium lacking compound. The constant treatment plate was allowed to incubate without washing. Plates were incubated for 10–14 days prior to ethanol fixation, staining with 0.1% crystal violet stain, and plaques counted using an Axio Observer.D1 microscope under 2.5× magnification.

Treatment during acute challenge studies—Adult (8–12 weeks old) female Balb/C mice were infected with 5,000 tachyzoites of the type II ME49 *hx::FLUC* line by i.p. injection. At 24 hr post-infection animals were dosed with compounds formulated in 25% PEG-PBS containing 5% DMSO, or 25% PEG-400-PBS- 5% DMSO alone, by oral gavage and treatment was continued for 6 days. Treated mice received one day 1, an initial loading

dose of compound **24** at 50 mg/kg in the morning, followed twelve hr later by a second dose of 25 mg/kg, and then 25 mg/kg BID for 5 additional days. Bioluminescence imaging (see below) was used to monitor infection from day 6 to 20, and weight loss and survival were tracked over the first 30 days. At the end of 30 days, tissue cysts in the brain were quantified by staining with *Dolichos biflorus* lectin that was labeled with FITC, and microscopic examination, as described previously⁵⁰. For samples where no cysts were observed (lower threshold = 40 per brain), residual infection was tested by bioassay into a naïve recipient. For bioassay experiments, 200 µL of brain homogenate was injected i.p. into a recipient *Ifngr1*^{-/-} mouse, which lack the ability to control parasite proliferation and readily succumb to infection³⁷.

Treatment during reactivation of chronic toxoplasmosis—To provide a model for treatment during reactivation of chronic infection, we used a modification of a previously published protocol^{38, 41}. Male and female *Ifngr1*^{-/-} mice were orally infected with 5 cysts of the type II ME49 *hx::FLUC* line, obtained from the brains of chronically infected wild type CD-1 mice. Animals were treated with sulfadiazine (0.25 g/L in the drinking water) from day 2–22. Two days (48 hr) after removal of the sulfadiazine, compound **24** formulated in 25% PEG-400-PBS containing 5% DMSO, or 25% PEG-400-PBS- 5% DMSO alone (control), were administered by oral gavage for a total of 8 days. One group of treated mice received one day 1, an initial loading dose of compound **24** at 50 mg/kg in the morning, followed twelve hr later by a second dose of 25 mg/kg, and then 25 mg/kg BID for 7 additional days. A second group of animals received compound **24** at 40 mg/kg BID for 8 days. Animals were monitored for weight loss, bioluminescence imaging, and survival for 30 days. At the end of 30 days, animals were examined for presence of cysts in the brain and by bioassay by inoculation of brain homogenate (200 µL of 1 ml) into a naïve recipient *Ifngr1*^{-/-} mouse, as described above. There were no differences in outcome associated with the sex of animals.

Bioluminescence imaging—Animals were monitored for bioluminescence using a Xenogen IVIS200 instrument and analyzed using the Xenogen Living Image software (Caliper Life Sciences). Mice were anesthetized using 2% isoflurane and injected i.p. with D-luciferin (Biosynth AG) at 150 mg/ mg just prior to imaging.

Statistical analyses

Mathematical and statistical analyses were conducted in Prism (GraphPad). IC₅₀ and EC₅₀ values were determined using normalized, log-transformed (conc.) data fit with nonlinear regression analysis based on sigmoidal dose-response curves with variable slope. For correlating IC₅₀ to EC₅₀ values, r² values were generated using linear regression analysis. Mean values for inhibition of bradyzoite plaque formation were analyzed using two-way ANOVA with Dunnett's correction for multiple comparisons. Survival curves were plotted as Kaplan Meier survival curves and significance determined by the Mantel-Cox test. Mean values for bioluminescence and weight loss were compared using Student's t-test with Holm-Sidak correction for multiple tests. The average numbers of cysts per brain were compared using a Mann-Whitney non-parametric test for non-normally distributed data with

unequal variance. For all test, a minimum value of $P = 0.05$ was considered significant and individual values are given in the figure legends.

Supplementary Material

Refer to Web version on PubMed Central for supplementary material.

Acknowledgments

We are grateful to Keliang Tang who performed the initial studies on enzyme kinetics and established the enzyme assays and to Martin John Rodgers for his early support of this project. We also thank John R. Walker of the Structural Genomics Consortium for verifying the crystallographic structures and for their deposition into the Protein Data Bank and the UCSF NMR Lab and QB3/Chemistry Mass Spectrometry Facility (University of California, Berkeley) for access to instrumentation for compound characterization. Supported by a grant from the NIH (AI094098 to K.M.S. and L.D.S.). The compounds reported here are the subject of patent applications filed by UCSF and Washington University.

Abbreviations Used

ANOVA	analysis of variance
β-gal	β -galactosidase
BID	bis in die (twice a day)
CDPK1	calcium dependent protein kinase 1
CNS	central nervous system
EC₅₀	50% effective concentration
ELISA	enzyme-linked immunosorbent assay
HAART	highly active anti-retroviral therapy
HFF	human foreskin fibroblast
HIV	human immunodeficiency virus
IC₅₀	50% inhibitor concentration
FLUC	firefly luciferase
SAR	structure activity relationship

References

1. Montoya JG, Liesenfeld O. Toxoplasmosis. *Lancet*. 2004; 363:1965–1976. [PubMed: 15194258]
2. Dennis AM, Napravnik S, Sena AC, Eron JJ. Late entry to HIV care among Latinos compared with non-Latinos in a southeastern US cohort. *Clin. Infect. Dis.* 2011; 53:480–487. [PubMed: 21844031]
3. Kiderlen TR, Liesenfeld O, Schurmann D, Schneider T. Toxoplasmic encephalitis in AIDS-patients before and after the introduction of highly active antiretroviral therapy (HAART). *Eur. J. Clin. Microbiol. Infect. Dis.* 2011; 30:1521–1525. [PubMed: 21491176]

4. Oliveira JF, Greco DB, Oliveira GC, Christo PP, Guimaraes MD, Oliveira RC. Neurological disease in HIV-infected patients in the era of highly active antiretroviral treatment: a Brazilian experience. *Rev. Soc. Bras. Med. Trop.* 2006; 39:146–151. [PubMed: 16699639]
5. Palella FJ, Delaney KM, Moorman AC, Loveless MO, Fuhrer J, Satten GA, Aschman DJ, Holmberg SD. The HIV Outpatient Study Investigators. Declining morbidity and mortality among patients with advanced human immunodeficiency virus infection. *N. Engl. J. Med.* 1998; 13:853–860.
6. Israelski DM, Remington JS. Toxoplasmosis in the non-AIDS immunocompromised host. *Curr. Clin. Top. Infect. Dis.* 1993; 13:322–356. [PubMed: 8397917]
7. Arantes TE, Silveira C, Holland GN, Muccioli C, Yu F, Jones JL, Goldhardt R, Lewis KG, Belfort R Jr. Ocular involvement following postnatally acquired *Toxoplasma gondii* infection in southern Brazil: A 28-year experience. *Am. J. Ophthalmol.* 2015; 159:1002–1012. e1002. [PubMed: 25743338]
8. Jacobson JM, Davidian M, Rainey PM, Hafner R, Raasch RH, Luft BJ. Pyrimethamine pharmacokinetics in human immunodeficiency virus-positive patients seropositive for *Toxoplasma gondii*. *Antimicrob. Agents Chemother.* 1996; 40:1360–1365. [PubMed: 8726001]
9. McCabe, RE. Antitoxoplasma chemotherapy. In: Joynson, DHM., Wreghitt, TG., editors. *Toxoplasmosis: a Comprehensive Clinical Guide*. Cambridge Univ. Press; Cambridge: 2001. p. 319-359.
10. Weiss, LM., Kim, K. Bradyzoite development. In: Weiss, LM., Kim, K., editors. *Toxoplasma gondii the Model Apicomplexan: Perspectives and Methods*. Academic Press; New York: 2007. p. 341-366.
11. Watts E, Zhao Y, Dhara A, Eller B, Patwardhan A, Sinai AP. Novel approaches reveal that *Toxoplasma gondii* bradyzoites within tissue cysts are dynamic and replicating entities in vivo. *MBio.* 2015; 6:e01155–01115. [PubMed: 26350965]
12. Lourido S, Shuman J, Zhang C, Shokat KM, Hui R, Sibley LD. Calcium-dependent protein kinase 1 is an essential regulator of exocytosis in *Toxoplasma*. *Nature.* 2010; 465:359–362. [PubMed: 20485436]
13. Ojo KK, Larson ET, Keyloun KR, Castaneda LJ, DeRoucher AE, Kinampudi KK, Kim JE, Arakaki TL, Murphy RC, Zhang L, Napuli AJ, Maly DJ, Verlinde CLMJ, Buckner FS, Parsons M, Hol WGJ, Merritt EA, Van Voorhis C. *Toxoplasma gondii* calcium-dependent protein kinase 1 is a target for selective kinase inhibitors. *Nat. Struct. Molec. Biol.* 2010; 17:602–607. [PubMed: 20436472]
14. Wernimont AK, Artz JD, Finerty P, Lin Y, Amani M, Allali-Hassani A, senisterra G, Vedadi M, Tempel W, Mackenzie F, Chau I, Lourido S, Sibley LD, Hui R. Structures of apicomplexan calcium-dependent protein kinases reveal mechanism of activation by calcium. *Nat. Struct. Molec. Biol.* 2010; 17:596–601. [PubMed: 20436473]
15. Manning G, Whyte DB, Martinez R, Hunter T, Sudarsanam S. The protein kinase complement of the human genome. *Science.* 2002; 298:1912–1934. [PubMed: 12471243]
16. Hui R, El Bakkouri M, Sibley LD. Designing selective inhibitors for calcium-dependent protein kinases in apicomplexans. *Trends Pharmacol. Sci.* 2015; 36:452–460. [PubMed: 26002073]
17. Bishop AC, Shah K, Liu Y, Witucki L, Kung C, Shokat KM. Design of allele-specific inhibitors to probe protein kinase signaling. *Curr. Biol.* 1998; 8:257–266. [PubMed: 9501066]
18. Liu Y, Bishop A, Witucki L, Kraybill B, Shimizu E, Tsien J, Ubersax J, Blethrow J, Morgan DO, Shokat KM. Structural basis for selective inhibition of Src family kinases by PPI. *Chem. Biol.* 1999; 6:671–678. [PubMed: 10467133]
19. Johnson SM, Murphy RC, Geiger JA, DeRocher AE, Zhang Z, Ojo KK, Larson ET, Perera BG, Dale EJ, He P, Reid MC, Fox AM, Mueller NR, Merritt EA, Fan E, Parsons M, Van Voorhis WC, Maly DJ. Development of *Toxoplasma gondii* calcium-dependent protein kinase 1 (TgCDPK1) inhibitors with potent anti-toxoplasma activity. *J. Med. Chem.* 2012; 55:2416–2426. [PubMed: 22320388]
20. Larson ET, Ojo KK, Murphy RC, Johnson SM, Zhang Z, Kim JE, Leibly DJ, Fox AM, Reid MC, Dale EJ, Perera BG, Kim J, Hewitt SN, Hol WG, Verlinde CL, Fan E, Van Voorhis WC, Maly DJ, Merritt EA. Multiple determinants for selective inhibition of apicomplexan calcium-dependent protein kinase CDPK1. *J. Med. Chem.* 2012; 55:2803–2810. [PubMed: 22369268]

21. Murphy RC, Ojo KK, Larson ET, Castellanos-Gonzalez A, Perera BG, Keyloun KR, Kim JE, Bhandari JG, Muller NR, Verlinde CL, White AC, Merritt EA, Van Voorhis WC, Maly DJ. Discovery of potent and selective inhibitors of calcium-dependent protein kinase 1 (CDPK1) from *Cryptosporidium parvum* and *Toxoplasma gondii*. ACS. Med. Chem. Lett. 2010; 1:331–335. [PubMed: 21116453]
22. Doggett JS, Ojo KK, Fan E, Maly DJ, Van Voorhis WC. Bumped kinase inhibitor 1294 treats established *Toxoplasma gondii* infection. Antimicrob. Agents Chemother. 2014; 58:3547–3549. [PubMed: 24687502]
23. Lourido S, Zhang C, Lopez MS, Tang K, Barks J, Wang Q, Wildman SA, Shokat KM, Sibley LD. Optimizing small molecule inhibitors of calcium-dependent protein kinase 1 to prevent infection by *Toxoplasma gondii*. J. Med. Chem. 2013; 56:3068–3077. [PubMed: 23470217]
24. Vidadala RS, Rivas KL, Ojo KK, Hulverson MA, Zambriski JA, Bruzual I, Schultz TL, Huang W, Zhang Z, Scheele S, DeRocher AE, Choi R, Barrett LK, Siddaramaiah LK, Hol WG, Fan E, Merritt EA, Parsons M, Freiberg G, Marsh K, Kempf DJ, Carruthers VB, Isoherranen N, Doggett JS, Van Voorhis WC, Maly DJ. Development of an orally available and central nervous system (CNS) reentrant *Toxoplasma gondii* calcium-dependent protein kinase 1 (TgCDPK1) inhibitor with minimal human ether-a-go-go-related gene (hERG) activity for the treatment of toxoplasmosis. J. Med. Chem. 2016; 59:6531–6546. [PubMed: 27309760]
25. Hanefeld U, Rees CW, White AJP, Williams DJ. One-pot synthesis of tetrasubstituted pyrazoles - proof of regiochemistry. J. Am. Chem. Soc. 1996; 0:1545–1552.
26. Schenone S, Radi M, Musumeci F, Brullo C, Botta M. Biologically driven synthesis of pyrazolo[3,4-d]pyrimidines as protein kinase inhibitors: an old scaffold as a new tool for medicinal chemistry and chemical biology studies. Chem. Rev. 2014; 114:7189–7238. [PubMed: 24873489]
27. Kwong FY, Buchwald SL. A general, efficient, and inexpensive catalyst system for the coupling of aryl iodides and thiols. Org. Lett. 2002; 4:3517–3520. [PubMed: 12323058]
28. Ley SV, Thomas AW. Modern synthetic methods for copper-mediated C(aryl)-O, C(aryl)-N, and C(aryl)-S bond formation. Angewandte Chem. 2003; 42:5400–5449.
29. Ma D, Cai Q. N,N-dimethyl glycine-promoted ullmann coupling reaction of phenols and aryl halides. Org. Lett. 2003; 5:3799–3802. [PubMed: 14535713]
30. Prim D, Campagne J-m, Andrioletti B. Palladium-catalysed reactions of aryl halides with soft, non-organometallic nucleophiles. Tetrahedron. 2002; 58:2041–2075.
31. Zaretski J, Matlock M, Swamidass SJ. XenoSite: accurately predicting CYP-mediated sites of metabolism with neural networks. J. Chem. Inform. Model. 2013; 53:3373–3383.
32. Bohm HJ, Banner D, Bendels S, Kansy M, Kuhn B, Muller K, Obst-Sander U, Stahl M. Fluorine in medicinal chemistry. Chembiochem. 2004; 5:637–643. [PubMed: 15122635]
33. Barnes-Seeman D, Jain M, Bell L, Ferreira S, Cohen S, Chen XH, Amin J, Snodgrass B, Hatsis P. Metabolically stable tert-butyl replacement. ACS Med. Chem. Lett. 2013; 4:514–516. [PubMed: 24900702]
34. Hicken EJ, Marmsater FP, Munson MC, Schlachter ST, Robinson JE, Allen S, Burgess LE, Delisle RK, Rizzi JP, Topalov GT, Zhao Q, Hicks JM, Kallan NC, Tarlton E, Allen A, Callejo M, Cox A, Rana S, Klopfenstein N, Woessner R, Lyssikatos JP. Discovery of a novel class of imidazo[1,2-a]pyridines with potent PDGFR activity and oral bioavailability. ACS. Med. Chem. Lett. 2014; 5:78–83. [PubMed: 24900776]
35. Shim HJ, Kim HI, Lee ST. The associated pyrazolopyrimidines PP1 and PP2 inhibit protein tyrosine kinase 6 activity and suppress breast cancer cell proliferation. Oncol. Lett. 2017; 13:1463–1469. [PubMed: 28454278]
36. Lourido S, Jeschke GR, Turk BE, Sibley LD. Exploiting the unique ATP-binding pocket of toxoplasma calcium-dependent protein kinase 1 to identify its substrates. ACS Chem. Biol. 2013; 8:1155–1162. [PubMed: 23530747]
37. Yap GS, Sher A. Effector cells of both nonhemopoietic and hemopoietic origin are required for interferon (IFN)-gamma- and tumor necrosis factor (TNF)-alpha-dependent host resistance to the intracellular pathogen, *Toxoplasma gondii*. J. Exp. Med. 1999; 189:1083–1091. [PubMed: 10190899]

38. Dunay IR, Heimesaat MM, Bushrab FN, Muller RH, Stocker H, Arasteh K, Kurowski M, Fitzner R, Borner K, Liesenfeld O. Atovaquone maintenance therapy prevents reactivation of toxoplasmic encephalitis in the murine model of reactivated toxoplasmosis. *Antimicrob. Agents Chem.* 2004; 48:4848–4854.
39. Zhang C, Lopez MS, Dar AC, Ladow E, Finkbeiner S, Yun CH, Eck MJ, Shokat KM. Structure-guided inhibitor design expands the scope of analog-sensitive kinase technology. *ACS Chem. Biol.* 2013; 8:1931–1938. [PubMed: 23841803]
40. Long AM, Zhao H, Huang X. Structural basis for the potent and selective inhibition of casein kinase 1 epsilon. *J. Med. Chem.* 2012; 55:10307–10311. [PubMed: 23106386]
41. Dunay IR, Chan WC, Haynes RK, Sibley LD. Artemisone and artemiside control acute and reactivated toxoplasmosis in the murine model. *Antimicrob. Agents Chemother.* 2009; 53:4450–4456. [PubMed: 19635951]
42. Minor W, Cymborowski M, Otwinowski Z, Chruszcz M. HKL-3000: the integration of data reduction and structure solution—from diffraction images to an initial model in minutes. *Acta Crystallogr. D Biol. Crystallogr.* 2006; 62:859–866. [PubMed: 16855301]
43. Bricogne, G., Blanc, E., Brandl, M., Flensburg, C., Keller, P., W, P., Roversi, P., Sharff, A., Smart, OS., Vonrhein, C., Womack, TO. BUSTER version 2.10.0. Cambridge, United Kingdom: Global Phasing Ltd; 2011.
44. Murshudov GN, Vagin AA, Dodson EJ. Refinement of macromolecular structures by the maximum-likelihood method. *Acta Crystallogr. D Biol. Crystallogr.* 1997; 53:240–255. [PubMed: 15299926]
45. Emsley P, Cowtan K. Coot: model-building tools for molecular graphics. *Acta Crystallogr. D Biol. Crystallogr.* 2004; 60:2126–2132. [PubMed: 15572765]
46. Davis IW, Leaver-Fay A, Chen VB, Block JN, Kapral GJ, Wang X, Murray LW, Arendall WB 3rd, Snoeyink J, Richardson JS, Richardson DC. MolProbity: all-atom contacts and structure validation for proteins and nucleic acids. *Nucleic Acids. Res.* 2007; 35:W375–383. [PubMed: 17452350]
47. Molecular Operating Environment (MOE), 2013.08. Chemical Computing Group ULC; Montreal, QC, Canada: 2017.
48. Fox BA, Falla A, Rommereim LM, Tomita T, Gigley JP, Mercier C, Cesbron-Delauw MF, Weiss LM, Bzik DJ. Type II *Toxoplasma gondii* KU80 knockout strains enable functional analysis of genes required for cyst development and latent infection. *Eukaryot. Cell.* 2011; 10:1193–1206. [PubMed: 21531875]
49. Tobin CM, Knoll LJ. A patatin-like protein protects *Toxoplasma gondii* from degradation in a nitric oxide-dependent manner. *Infect. Immun.* 2012; 80:55–61. [PubMed: 22006568]
50. Wang ZT, Harmon S, O'Malley KL, Sibley LD. Reassessment of the role of aromatic amino acid hydroxylases and the effect of infection by *Toxoplasma gondii* on host dopamine. *Infect. Immun.* 2015; 83:1039–1047. [PubMed: 25547791]
51. Eid S, Turk S, Volkamer A, Rippmann F, Fulle S. KinMap: a web-based tool for interactive navigation through human kinome data. *BMC Bioinform.* 2017; 18:16.

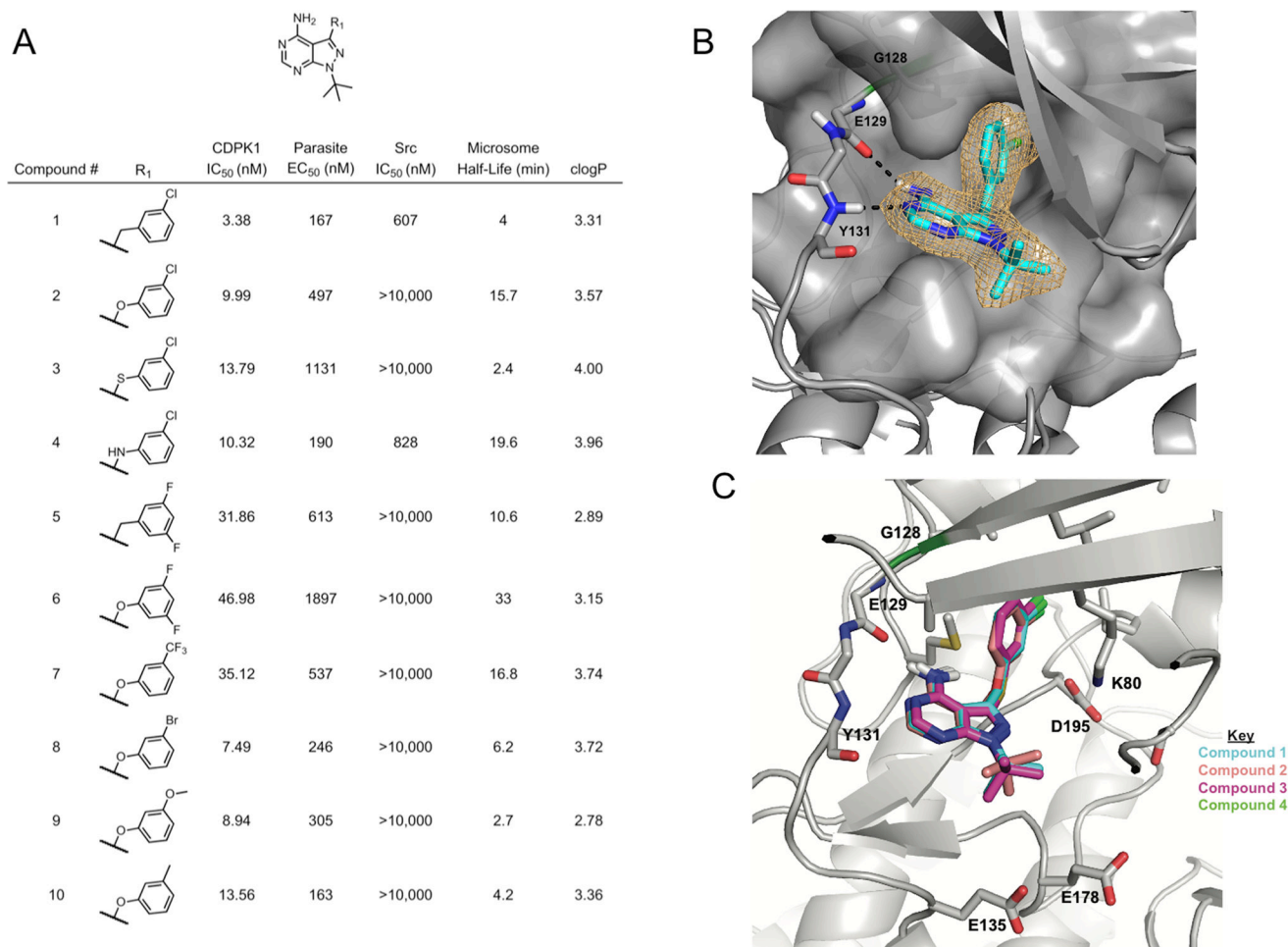
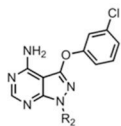


Figure 1.

A



Compound #	R ₂	CDPK1 IC ₅₀ (nM)	Parasite EC ₅₀ (nM)	Src IC ₅₀ (nM)	Microsome (min)	clogP
2		9.99	497	>10,000	15.7	3.57
11		190.6	>10,000	>10,000	>60	1.45
12		118.6	4091	>10,000	>60	2.01
13		14.15	437	>10,000	>60	2.57
14		73.09	1821	>10,000	>60	2.57
15		271.9	>10,000	>10,000	14	2.80
16		218.5	2653	>10,000	14	2.59

B

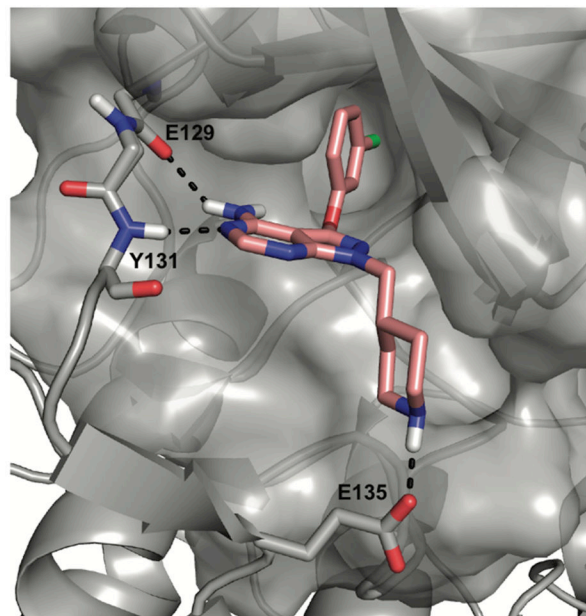
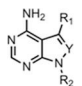


Figure 2.

A

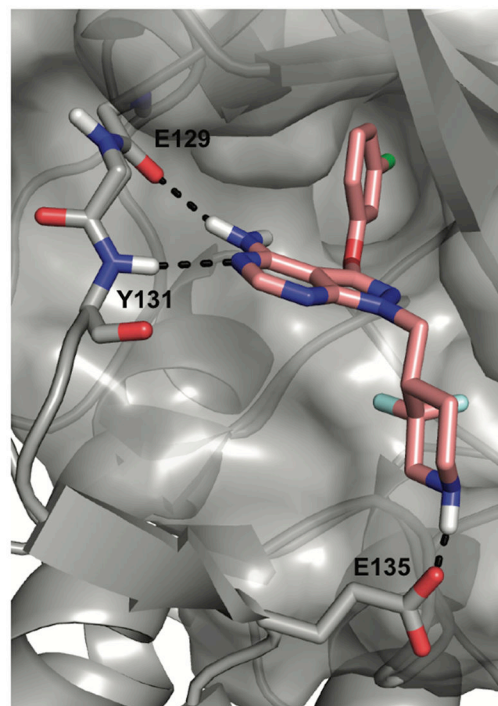


Compound #	R ₁	Y	R ₂	CDPK1 IC ₅₀ (nM)	Parasite EC ₅₀ (nM)	Src IC ₅₀ (nM)	Microsome (min)	clogP
13		N		14.15	437	>10,000	>60	2.57
17		N		14.53	799	>10,000	>60	2.31
18		N		19.2	242	>10,000	11	3.00
19		N		517	729	>10,000	26	2.78
20		N		16.4	3476	901	20	2.95
21		N		173	5976	>10,000	>60	1.88
22		N		67.5	2979	>10,000	>60	2.71

23		C		13.53	367	>10,000	9.6	3.82

24		N		10.9	264	>10,000	8.8	2.85
25		N		77.5	1803	>10,000	>60	3.01
26		N		95.3	>10,000	>10,000	>60	1.22
27		N		10.2	1004	>10,000	11	3.45
28		N		47	1000	>10,000	2.5	3.28

Figure 3.

B

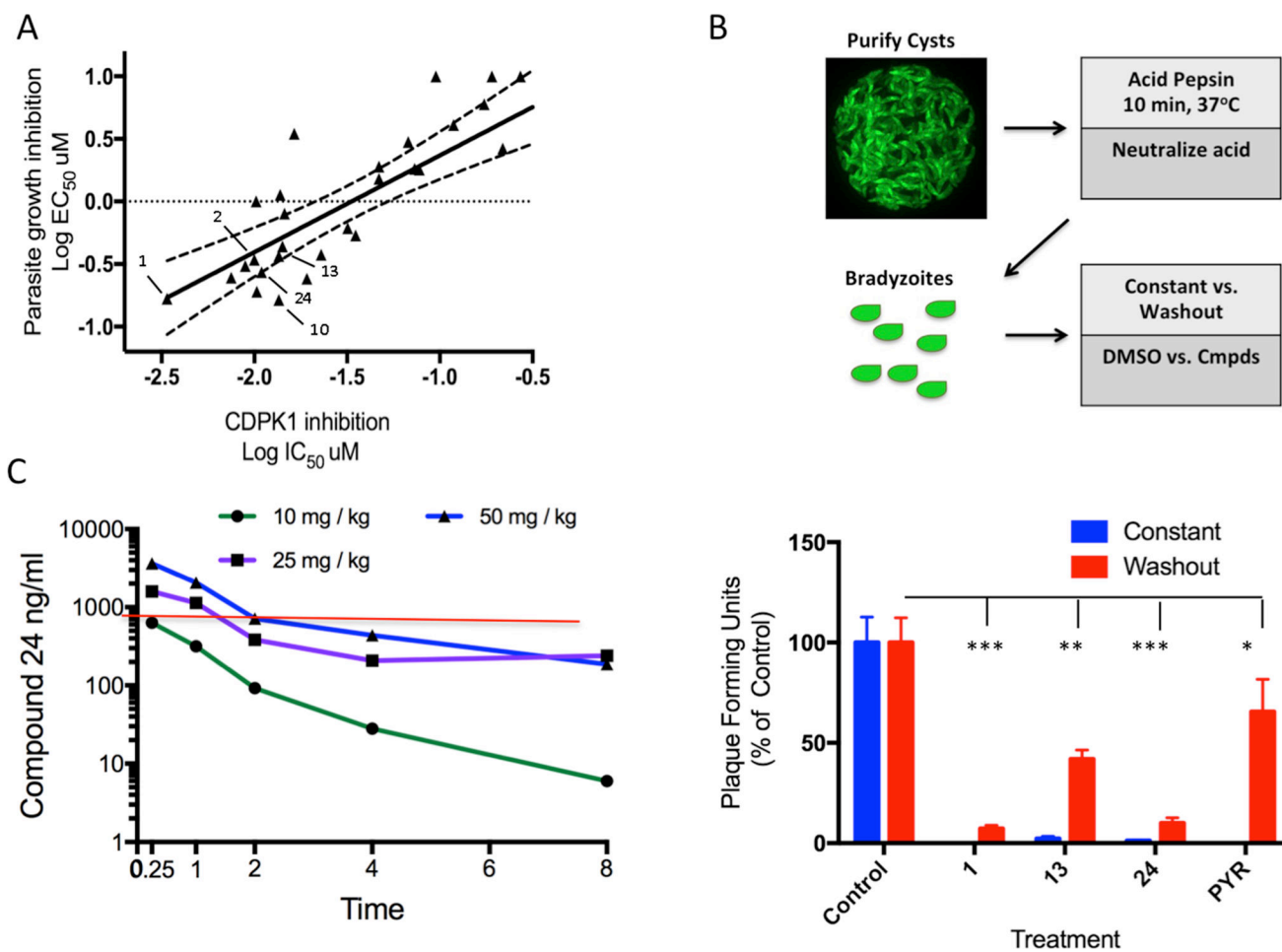


Figure 4.

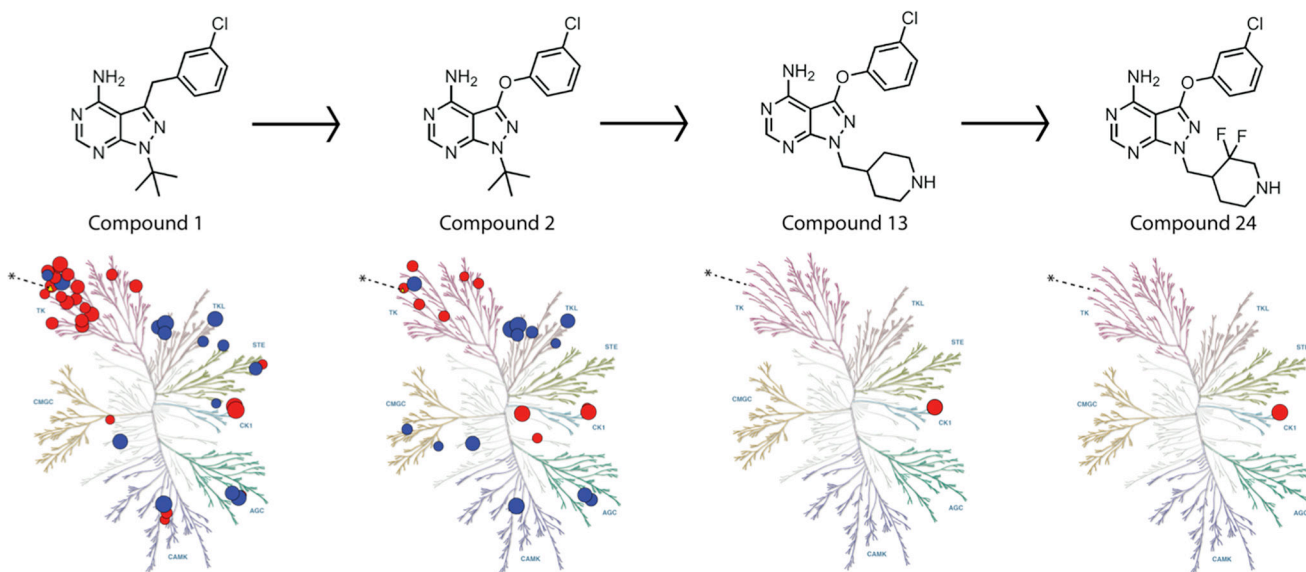


Figure 5.

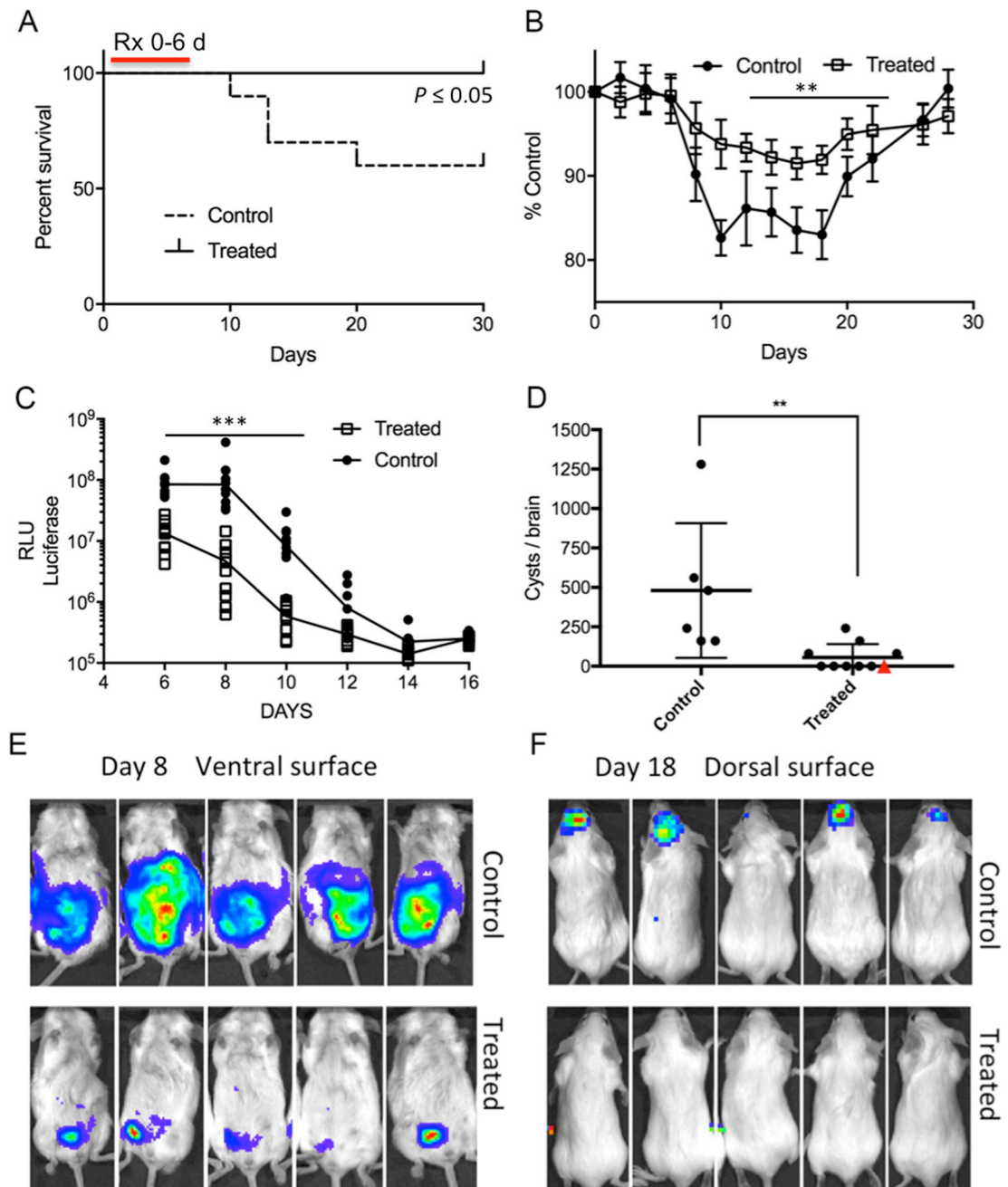


Figure 6.

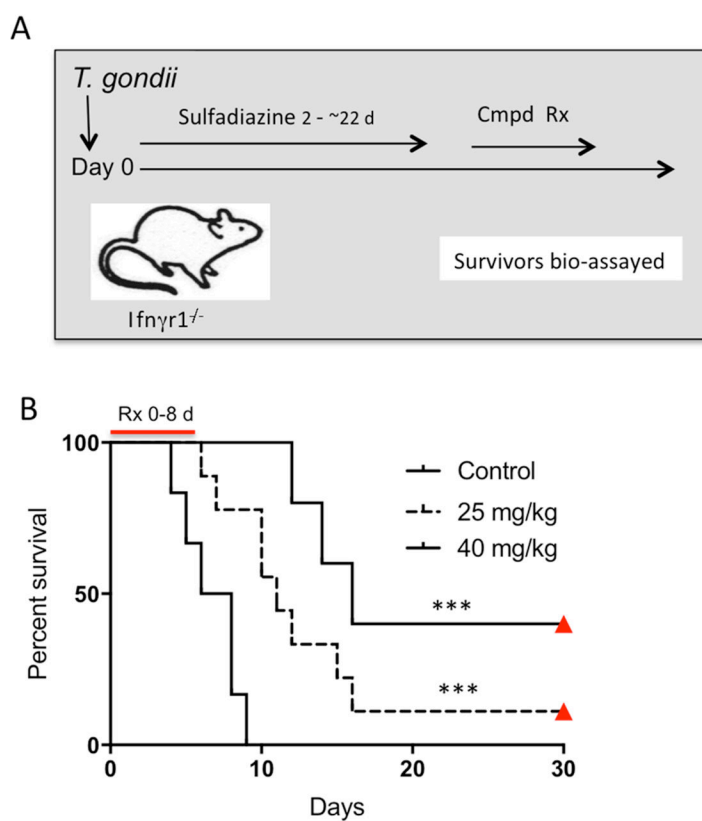
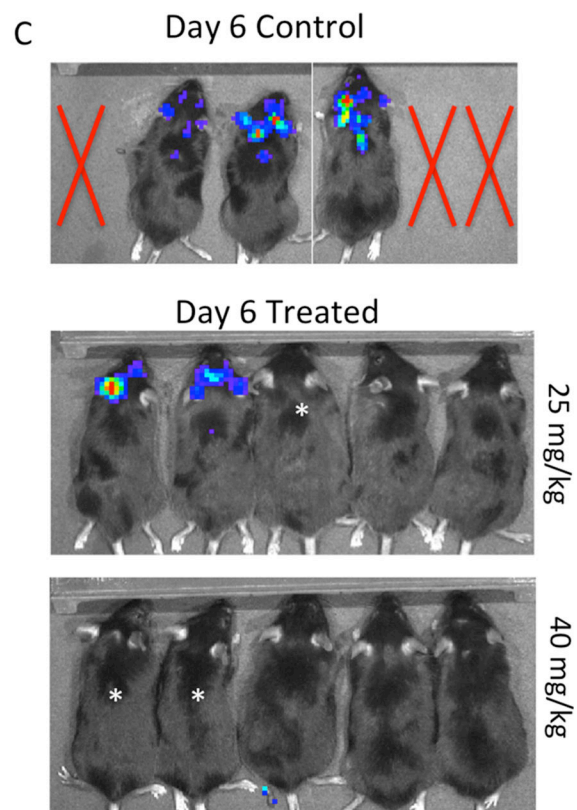
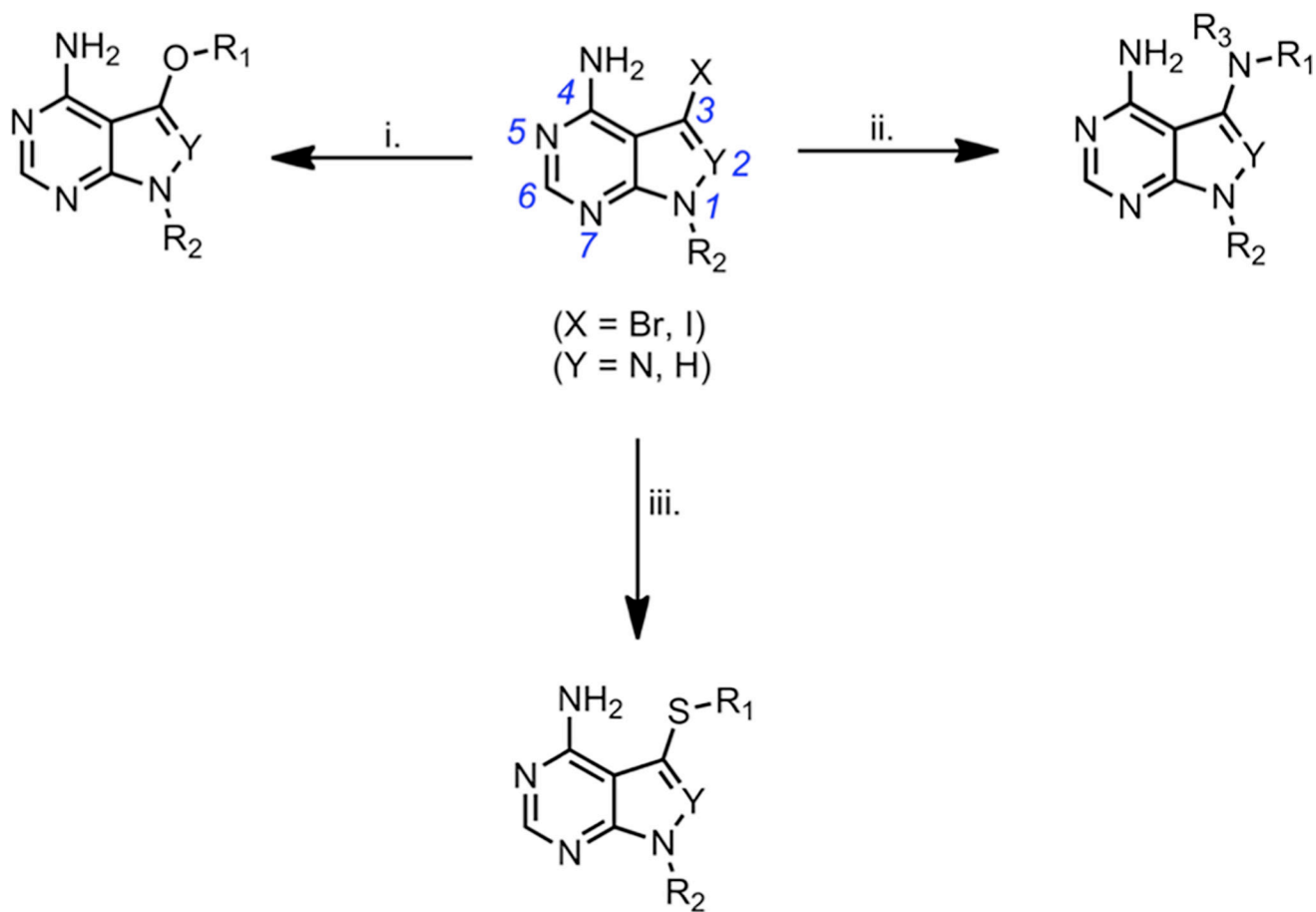


Figure 7.





Scheme 1.

Table 1

Physical parameters, metabolic stability, efflux, and toxicity of select compounds

Cmpd	ClogP ₁	tPSA	pKa	Protein binding	Papp 10 ⁻⁶ cs/s A to B ²	Papp 10 ⁻⁶ cs/s B to A ³	Efflux ratio ⁴	Microsomes ⁵ CL _{int} ⁴ mL / min/mg	Cell toxicity ⁶
1	3.15	66.34	-	99.2%	42.9	28.7	0.7	0.452	>10 μM
2	3.48	75.57	-	99.8%	34.8	30.6	0.9	0.281	>10 μM
10	3.41	75.57	-	98.4%	15.0	14.6	1.0	1.240	>10 μM
13	2.57	87.6	10.4	73.5%	1.07	9.58	8.9	0.019	>10 μM
24	3.0	87.6	7.1	88.3%	22.8	21.2	0.9	0.694	>10 μM
18	3.25	78.37	10.4	87.5%	2.76	25.6	9	0.072	>10 μM
28	3.57	78.37	7.1	91.8%	27.1	25.3	.9	0.887	>10 μM

¹ Determined in Chemdraw Ultra 12.0, PerkinElmer Informatics² Apparent permeability (Papp), apical to basolateral (A-B)³ Apparent permeability (Papp) basolateral to apical (B-A)⁴ Papp (B to A) / Papp (A to B)⁵ CL_{int} = k/P, where k is the elimination rate constant and P is the protein concentration in the assay⁶ Mouse liver microsomes⁷ Inhibition of replication of human HFF cells

Table 2

In vivo pharmacokinetic properties based on plasma levels of select compounds

Cmpd	Route	Dose mg/kg	Tmax hr	Co/Cmax ¹ ng/ml	AUC ^{last} ng/ml hr	AUC _{inf} ² ng/ml hr	T _{1/2} hr	CL ² ml/min/kg	V _{ss} ³ L/kg	%F ⁴
1	iv	3	-	6892.94	1075.29	1081.76	2.06	46.22	1.09	-
	po	10	0.25	585.42	918.80	930.88	-	-	-	26
2	iv	3	-	5471.09	1146.49	1149.99	1.56	43.48	1.10	-
	po	10	0.25	1136.36	1172.75	1279.20	-	-	-	31
10	iv	3	-	2741.80	619.33	625.04	1.74	80	2.32	-
	po	10	0.25	76.69	85.47	91.42	-	-	-	4
13	iv	3	-	535.79	449.57	523.99	3.68	95.42	19.59	-
	po	10	2.00	182.56	757.85	891.24	-	-	-	51
24	iv	3	-	1205.19	975.90	988.58	1.56	50.58	3.68	-
	po	10	0.25	1048.80	3058.44	3547.95	-	-	-	94

¹ C_{max} for po route, C₀ (initial conc.)

² CL, clearance

³ V_{ss} steady-state volume of distribution

⁴ Oral availability determined from AUC_{last}